RSC Applied Polymers

ROYAL SOCIETY OF CHEMISTRY

PAPER

View Article Online
View Journal

Cite this: DOI: 10.1039/d5lp00277j

The effect of crystallinity of HDPE precursor film on the properties of the resultant radiation-grafted anion-exchange membranes

Siân A. Franklin, Carol Crean and John R. Varcoe *

An advantage of using pre-irradiation grafting for the synthesis of anion exchange membranes (AEMs) is it allows the use of pre-made commercial substrates as the precursor film. To consider scaling-up radiation grafted AEM (RG-AEM) production, it is vital to understand how variation in manufacturing of the precursor film impacts the final RG-AEM properties. In this study, it is shown that commercially supplied 10 m length rolls of high density polyethylene (HDPE) films vary in crystallinity both within and between rolls (to a maximum of 17%). Consequently, the degree of grafting (DoG), ion exchange capacity (IEC), and conductivity of the resultant RG-AEMs were impacted. A negative correlation between crystallinity and DoG and conductivity was observed with Pearson R values of −0.5 and −0.6, respectively. A threshold effect was observed around 82% crystallinity: above this crystallinity value, the variations in DoG and conductivity decreased. A similar effect was also observed for IEC at a crystallinity threshold of approximately 81%. These findings suggest that fabrication of consistent property RG-AEMs requires a precursor film crystallinity of greater than 81%. Finally, a positive correlation was observed between crystallinity and water uptake (WU, Pearson R = +0.7), with more crystalline precursor film resulting in increased WU being observed in the resultant RG-AEMs. This counter intuitive correlation shows that alongside variations in bulk degrees of crystallinity values (considered in this paper), investigations will be required to account for crystallite size and distributions that can impact the hydration channel morphology within the RG-AEMs.

Received 2nd September 2025,
Accepted 23rd October 2025

DOI: 10.1039/d5lp00277j

rsc.li/rscapplpolym

Background and context

Anion exchange membranes (AEMs) are electrically insulating polymers that selectively transport anions through the membrane *via* cationic head groups that are (typically) covalently bound to the polymer chains. They are integral to a number of emerging technologies including alkaline membrane fuel cells (AEMFC), anion exchange membrane electrolysers (for both H_2 generation and CO_2 electroreduction) and (reverse) electrodialysis.[1–3] Methods for preparing AEMs include classical polymerisations (with or without post functionalisation such as chloromethylation and bromination), pore filling, and grafting (commonly initiated using atom-transfer radical polymerisation, plasma, or radiation).[4–7]

Pre-irradiation grafting uses high-energy radiation, to form active (initiation) sites on a base polymer *via* bond homolysis, followed by radical chain-growth propagation of a monomer to form grafted side chains. Scheme 1 shows the synthesis reaction of a typical radiation-grafted (RG) AEM using high-density polyethylene (HDPE) as the precursor film, vinylbenzyl chloride (VBC) monomer, and trimethylamine (TMA) as the post-grafting amination/quaternisation agent.[8] The grafting stage of the reaction proceeds *via* the widely reported grafting front mechanism, where the monomer initially reacts at the surfaces of the film, after which the grafting moves inward into the film core until a bulk uniform grafting is achieved.[9]

Pre-irradiation grafting is advantageous as it allows large batches of less reactive polymers, fabricated to commercial tolerances and thicknesses, to be functionalised with a large range of chemistries. This allows AEMs to be tailored to multiple applications; *e.g.*, trimethylammonium-type AEMs made from thin 10 μm HDPE films are tailored for high performance

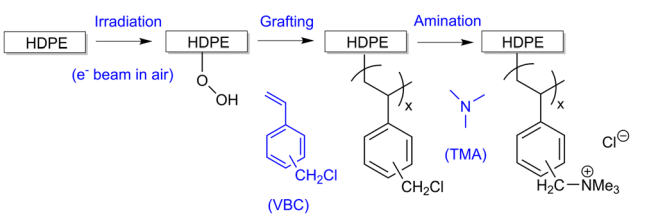

Scheme 1 An outline of the synthesis of RG-AEMs using HDPE precursor film that is subsequently grafted with VBC and aminated with TMA.

School of Chemistry and Chemical Engineering, The University of Surrey, Guildford, GU2 4DG, UK. E-mail: j.varcoe@surrey.ac.uk, sianafranklin@outlook.com

AEMFCs,[10] whilst *N*-methylpiperidinium-type AEMs made from thicker (25 μm) poly(ethylene-tetrafluoroethylene) (ETFE) films are better for CO_2 electrolysis cells.[11]

The microstructure, including the degree of crystallinity, crystallite size, and orientation are important properties of the precursor film that can dictate the structure, morphology, and properties of the final grafted and functionalised membranes.[12–15] This has been shown for RG-proton exchange membranes (RG-PEM). Walsby *et al.* showed a linear relationship between the crystallinity of partially fluorinated precursor films with the water uptake of the fabricated RG-PEMs;[16] the base films with a higher crystallinity were shown to be more dimensionally stable, a result of crystalline regions restraining swelling. In 2016, Sproll *et al.* examined the microstructure of two commercial partially-fluorinated ETFE films, where despite the levels of crystallinity being similar, small angle scattering experiments revealed the crystallite size differed between suppliers.[12] The RG-AEM prepared from the ETFE containing larger crystallites had higher H^+ conductivity and increased durability.

Few studies have focused on the impact of precursor film microstructure on the properties of RG-AEMs. In 2019 however, Wang *et al.* reported an increase in fuel cell performance from 2.0 mW cm^{-2} to 2.6 mW cm^{-2} at 80 °C in a H_2/O_2 AEMFC, as a result of changing the base film used from less-crystalline (more branched) low-density polyethylene (LDPE) to higher crystallinity HDPE.[10]

During the synthesis of RG-membranes, the microstructure of the polymer films is changed due to numerous processing parameters. The significantly high energy from irradiation (compared to the electron binding energy in the polymer) results in bond scissions, creating polymer bound free radicals (and small molecule by products); additional processes occur including crosslinking, peroxidation (if the process is conducted in air – Scheme 1), and chain-transfer/termination.[19] The extent of these processes, and how they change the intrinsic nature of the polymers, will be influenced by dose, temperature and reaction gas (inert or O_2 containing).[17–20] Subsequent grafting, *i.e.* polymerisation of monomers into the amorphous base film domains, tends to disrupt the crystalline phases, whilst the post-grafting introduction of ionic groups results in microphase separation between the hydrophobic and hydrophilic domains in the resulting RG-ion-exchange membranes.[7,21,22]

Due to their proprietary nature, a drawback of using commercial polymers as base films for the fabrication of RG-membranes is the lack of detailed information available; apart from the commonly declared density, information on processing conditions, crystallinity, and the additives used are generally not stated. The aim of this study is to measure the variation of crystallinity within a commercial roll of HDPE and determine if this variation affects a select range of properties of the resultant RG-AEM. It is worth considering that the influences from different processing parameters may mask the impact of subtle variations in crystallinity. This study builds towards the knowledge needed for the scale-up of RG-AEMs that is mandatory for larger batch production where the RG-AEM properties are reproducible and consistent.

Experimental

Materials and chemicals

Two rolls of HDPE film (10 m × 0.6 m) with a thickness of 10 μm were purchased from Goodfellows (product code ET32-FM-000110) and used to map variation in crystallinity. For RG-AEM synthesis, VBC monomer (*meta*-/*para*-isomer mixture, stabilised with 4-*tert*-butylcatechol inhibitor, ONP and *o*-nitrocresol) was purchased from TCI (product code C0767) and the inhibitor was removed in a column using aluminium oxide purchased from Merck. Toluene (≥99.5% purity), 1-octyl-2-pyrrolidone (98% purity), aqueous trimethylamine solution (TMA, 45 wt%), and NaCl (>99% purity), were purchased from Merck and used as received. Deionised (DI, grade II) water was used during the grafting and washing stages of the synthesis, whilst ultra-pure water (UPW) with a resistivity of 18.2 MΩ cm was used in the final ion-exchange and analytical experiments.

Sampling of the commercial rolls for property measurements

For the density measurements, three samples (15 cm length × 10 cm width) were taken at 1 m horizontal intervals along both commercial rolls (Fig. 1). Adjacent 15 cm × 10 cm samples were then prepared for the irradiation and subsequent synthesis of RG-AEMs.

Density measurements

The 15 cm × 10 cm samples were each pressed into $\frac{1}{4}$ inch pellet form at room temperature using a Specac manual hydraulic press (3 tonnes for 4 min). Each pellet was then placed in a 5 cm^3 sample holder and the density was measured using an Accupyc II 1345 pycnometer operating with He. For each sample, 10 measurements were taken. Crystallinity (X_c) was calculated using eqn (1):

$$X_c = \frac{\rho_c(\rho - \rho_a)}{\rho(\rho_c - \rho_a)} \quad (1)$$

where ρ is the density of the measured sample, ρ_a is the theoretical density of a 100% amorphous polyethylene (PE) sample (0.85 g cm^{-3}) and ρ_c is the theoretical density of a 100% crystalline PE sample (1.00 g cm^{-3}).[23]

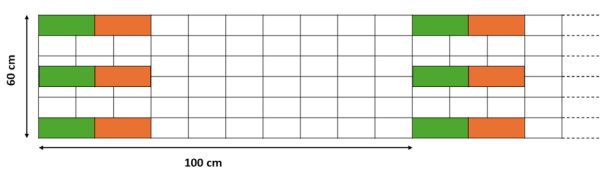

Fig. 1 A cartoon depicting the sample locations within the 60 cm × 10 m commercial rolls. The green rectangles denote the areas used to calculate crystallinity (*via* density measurements), whilst the orange rectangles show the area used for the synthesis of the RG-AEMs. These samples were taken at every 1 m intervals along the roll.

Synthesis of RG-AEMs[24]

Using a Rhodotron 80 kW, 10 MeV vertical electron beam (Sterigenics, Denmark), the 15 cm × 10 cm samples (cut from areas adjacent to the samples used for the above density measurements, Fig. 1) were irradiated in air at room temperature *via* multiple 10 kGy passes until a total dose of 100 kGy was applied (using 5 min rest periods between each pass to prevent sample overheating). Once irradiated, the film samples were returned to Surrey packed in dry ice (<2 days transit), where they were then stored at −40 ± 2 °C until required.

For grafting, each weighed irradiated film sample was placed in a N_2-pre-purged grafting solution containing 94 vol% DI water, 5 vol% VBC, and 1 vol% 1-octyl-2-pyrrolidone. The mixture was N_2-purged at 0 °C for 1 h and then placed in a pre-heated water bath (50 °C) for a further 4 h. The inert-gas purge was maintained throughout the grafting process. The grafted membrane samples were then washed in toluene to remove any homopolymer (poly(VBC) that was not covalently bound to the HDPE) after which they were dried overnight in air at room temperature. The degree of grafting (DoG) of each intermediate grafted HDPE sample was calculated using eqn (2):

$$\mathrm{DoG} = \left(\frac{m_g - m_i}{m_i}\right) \times 100\% \quad (2)$$

where m_i is the mass of the initial sample (after e^- beaming) and m_g is the mass of the grafted sample after drying.

To convert to the anion-conducting form (RG-AEM), each grafted membrane sample was submerged in excess aqueous trimethylamine (45 wt%, *ca.* 1 L) for 24 h, after which they were thoroughly washed in DI water at room temperature and then heated at 60 °C in DI water for 1 h. Ion exchange was completed by immersing the as-fabricated RG-AEM samples in aqueous NaCl (1.0 M) solution for 1 h (with replacement of the solution at least 3 times during this 1 h period), after which they were soaked in UPW for at least 1 h (with fresh replacements of UPW until no excess Cl^- ions remained). The pristine Cl^--form RG-AEM samples were then stored in UPW in plastic bottles until required for further characterisation.

Determination of the ion-exchange capacity (IEC)

For each RG-AEM sample, three replicate IEC measurements were completed. For each determination of IEC, the sub-sample was dried in a vacuum oven at 50 °C for 4 h before being weighed (m_d) and placed in 20 mL aqueous $NaNO_3$ solution (2.4 M) for 16 h. The solution (containing the sub-sample) was acidified with 2 mL HNO_3 (2 M) before being titrated with aqueous $AgNO_3$ titrant (0.02 M – NIST traceable volumetric standard supplied by Fisher with concentration tolerance factors between 0.997–1.003) using a Metrohm 848 Titrino plus autotitrator equipped with an Ag-titrode (Cl^--ion-selective electrode). Prior to each set of IEC determinations, the autotitrator calibration was checked by titrating blank solutions (three repeats) containing standardised NaCl solution (0.1000 M) added to 20 mL of aqueous $NaNO_3$ solution (2.4 M) and 2 mL of HNO_3 (2 M); typical IEC errors for these blank solutions were <1%. Each IEC value was calculated using eqn (3), where the end point volume (E_p) was taken as the maxima in the first differential plot of Ag electrode potential *vs.* titrant volume.[24]

$$\mathrm{IEC} = \frac{E_p \times [\mathrm{AgNO_3}]}{m_d} \quad (3)$$

The titrations of roll 1 occurred before those of roll 2 and the group transitioned to an updated method for roll 2 (reducing titration uncertainties). Table 1 provides the details of the two methods used.

Conductivity

To measure the in-plane Cl^- conductivities, strips of each RG-AEM sample were cut (4 cm × 1 cm) and placed into a BekkTech BT-112 4-probe conductivity test cell (supplied by Alvatek UK). The cell was then submerged in UPW at 60 °C and an alternating current (10 mV amplitude) was applied between 1 Hz and 100 kHz using a Solartron 1260/1287 impedance analyser. The low-frequency intercept along the real-axis in the obtained Nyquist plot, was taken as the resistance value (R/Ω). The conductivity (σ/S cm^{-1}) was calculated using eqn (4):

$$\sigma = \frac{l}{R \cdot w \cdot t} \quad (4)$$

where l is the distance between the Pt sense electrodes (0.425 cm), t and w are the thickness and width of the sample, respectively.

Water uptake

Gravimetric water uptakes were determined for each Cl^--form RG-AEM sample (5 × 5 cm) at room temperature as calculated using eqn (5):

$$\mathrm{WU} = \left(\frac{m_h - m_d}{m_d}\right) \times 100\% \quad (5)$$

where m_h is the hydrated mass of the sample after excess surface water was quickly removed with filter paper (within 1 min of being removed from the storage UPW), and m_d is the dehydrated mass sample, where the sample was dried in a vacuum oven at 50 °C for 4 h. Measurements were repeated 3 times for each sample.

Table 1 Difference in titration method between roll 1 and 2

	Roll 1	Roll 2
Sub sample size	2 cm × 2 cm	5 cm × 5 cm
Equivalence point titration (ET) method	Monotonic (MET)	Dynamic (DET)
Dispensing burette	20 mL	5 mL
NaCl volume added during blank measurement	2.0000 mL	0.5000 mL
Approximate titration time	1 h	5 min

Results and discussion

Crystallinity variation within commercially supplied HDPE

Three samples (15 cm × 10 cm) were taken at every 1 m horizontal interval along two 10 m commercial rolls. The bulk crystallinity for each sample was calculated using density measurements (eqn (1)). Density is a bulk measurement which uses a larger sample size (*ca.* 100 mg) compared to DSC (*ca.* 10 mg), hence this method allowed a more averaged crystallinity to be found at each location. This data was used to produce a low-resolution map to show the inter- and intra-roll changes in crystallinity (Fig. 2). A gradient of increasing crystallinity was observed moving along roll 2 with meter 1 (M1) having lower crystallinity values compared to M10. The observed gradient could be attributed to a change in cooling rate during the production process, which has been shown to impact crystallinity.[25,26] Conversely, roll 1 does not show a clear trend throughout the roll. Despite the commercial rolls being from the same supplier, using the same production method, the data supports the expectation that there are unavoidable variations in the manufacturing process (within the fabrication of a single roll and across different production dates). This leads to natural variations in the properties of the HDPE at different locations of a single roll and between different rolls, all of which can affect the radiation-grafting levels achieved (affecting grafting homogeneity and predictability).

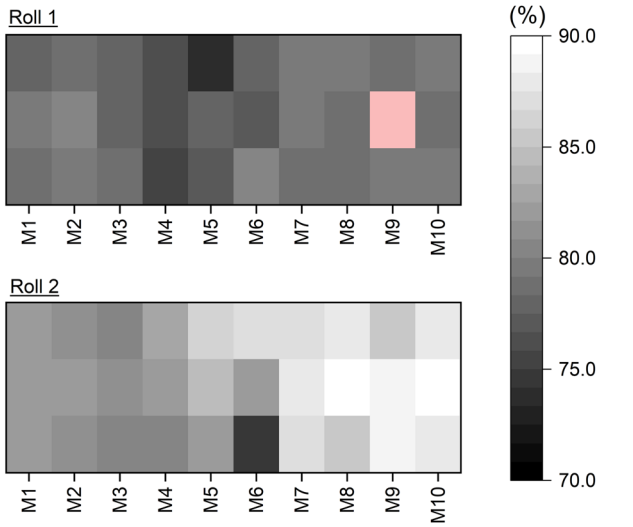

Fig. 2 Low resolution maps showing the variation in crystallinity along and between two commercial HDPE rolls supplied by Goodfellows. The pink sample in roll 1 signifies a sample that was lost before analysis.

When HDPE crystallinities were presented in a box plot (Fig. 3a) it was observed that roll 1 had a much smaller spread of crystallinity (74–81% range) compared to roll 2 (75–91% range). A two-sample *t*-test with welch correction (95% confidence level) was conducted, where roll 1 with a crystallinity of 78.4 ± 1.5% was shown to be significantly different from roll 2 (84.3 ± 3.7%): $t(39) = -8.0$ and $p = 9.6 \times 10^{-10}$. All crystallinity values were above 70% as expected for HDPE, which is defined as having a density greater than 0.944 g cm^{-3} (which translates to a crystallinity of 66%).

Fig. 3b shows the measured variation in crystallinity across both rolls and the standard deviation (narrow grey zone) associated with each measurement (n = 10 repeat measurements on each sample). The variation in the measured crystallinity is shown to be larger than the error associated with the measurement technique. This confirms that the variations observed both within and between the rolls is genuine. An interesting inflection was observed where not many samples were recorded with crystallinities in the range 83–86%.

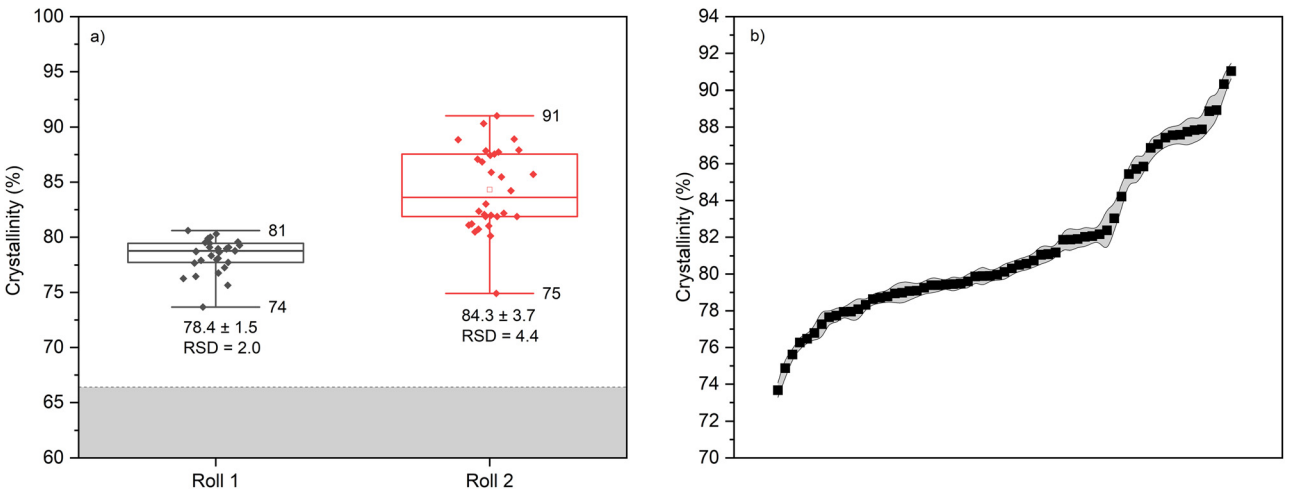

Fig. 3 Box plot showing the measured variation in crystallinity between rolls 1 and 2. The area shaded grey shows the degree of crystallinities threshold for PE (defined high density > 0.944 g cm^{-3}). (b) The mean crystallinities of the samples (across all rolls) arranged in order of increasing crystallinity (left to right) with the sample standard deviations (n = 10 repeat measurements on each sample) given as the grey zone.

Impact of crystallinity on VBC-grafting levels

The disadvantage of using density measurements to calculate crystallinity is that the technique is destructive; consequently, the specific sample used to determine crystallinity cannot then be used for radiation-grafting and AEM synthesis. Therefore, samples from directly adjacent areas (connected to the samples used for crystallinity determinations) were irradiated and grafted. This experiment required the assumption that the crystallinities between adjacent sites were comparable. To check the validity of this assumption, density measurements were taken between adjacent squares at different locations along roll 2 (selected as it showed the most intra-roll variation); the difference in crystallinity between adjacent squares was then calculated. The average difference in crystallinity between adjacent sample pairs was small at 1.9% (n = 8 pairs).

Fig. 4a shows a box plot with measured DoG values (eqn (2)) for the grafted membranes produced from roll 1 and roll 2. Interestingly, roll 1, with the smallest variations in HDPE degrees of crystallinity, had a larger spread of DoG values: a range of 156–235% (*cf.* roll 2 with a range of 169–225%). The average DoG for roll 1 was 207 ± 20% and found to be statistically different (using a two-sample t-test with welch correction, 95% confidence level) from roll 2 with a DoG of 187 ± 14%, where $t(48) = 4.4$ and $p = 6.9 \times 10^{-5}$.

Fig. 4b plots the HDPE crystallinity values of each sample *vs.* the DoG values of the directly adjacent grafted samples. A negative correlation is observed with higher DoG values being produced in samples adjacent to areas of lower crystallinities (Pearsons R value = −0.5). This is consistent with prior reports that grafting predominantly occurs in the amorphous zones; grafting initially occurs in the amorphous region of the base

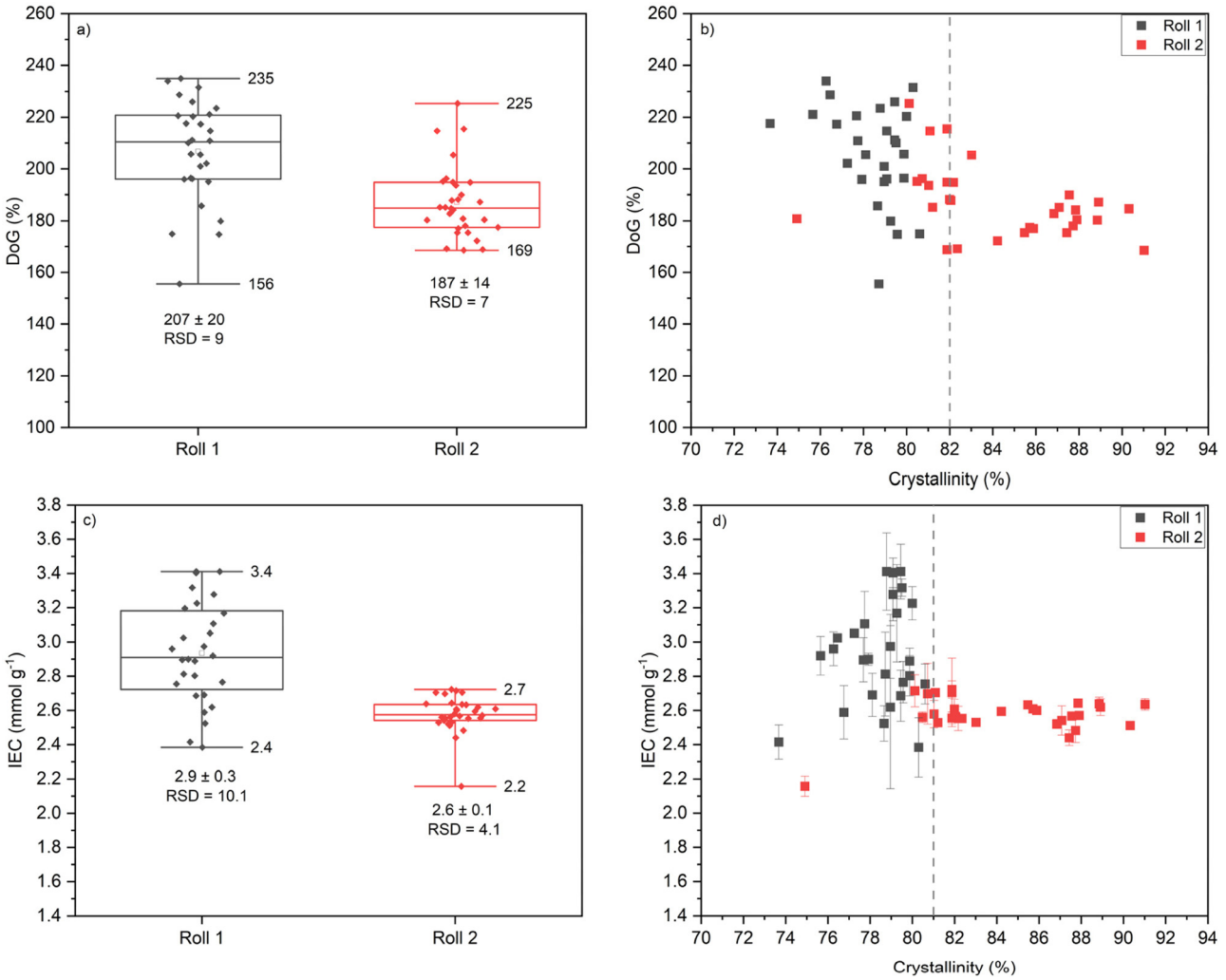

Fig. 4 (a) Box plot showing the variation in the DoG between commercial roll 1 and 2. (b) Scatter plot showing the relationship between crystallinity and DoG where the black squares indicate values from roll 1 and the red squares shows values obtained from roll 2. The dashed line at 82% marks the threshold at which crystallinity appears to no longer have an impact on the DoG. (c) Box plot showing the variation in the IEC between commercial roll 1 and 2. (d) Scatter plot showing the relationship between crystallinity and IEC. Similar to 4b, the dashed line at 81% crystallinity marks the threshold at which crystallinity no longer impacts the IEC.

films, whilst radicals trapped at the interface of the amorphous/crystalline region are slowly released, resulting in the gradual grafting of the crystalline phase.[27,28] However, there is a perceptible threshold effect at *ca.* 82% crystallinity, where higher crystallinities do not lead to any significant decrease in DoG values (to the right of the dashed line in Fig. 4b).

Impact of crystallinity on RG-AEM properties

The grafted samples were subsequently aminated with trimethylamine to yield benzyltrimethylammonium-type RG-AEM samples. After ion-exchange to the pure Cl^- form, the following properties were measured: IEC, WU, and in-plane conductivity (σ). The high IECs, conductivities and swelling values observed for the RG-AEMs are indicative of complete grafting and amination through the AEM, as opposed to only a surface reaction occurring. Raman microscopy confirmed this assumption with cross section analysis demonstrating homogenous amination throughout the thickness of the membrane (see SI Fig. S1). SEM and photography was subsequently used to observed surface RG-AEM morphology, which showed surface cracks and folds on the 10–100 nm level, but no significant macro defects observed (see SI Fig. S2–S4).

Fig. 4c shows a box plot for the IEC values obtained for each roll, with some similarities to the DoG data in Fig. 4a. A larger variance in IEC along with a higher mean IEC was observed for roll 1 (2.9 ± 0.3 mmol g^{-1}) compared to roll 2 (2.6 ± 0.1 mmol g^{-1}). A two-sample *t*-test (with welch correction, 95% confidence level) showed a significant difference between the mean IECs where $t(33) = 6.0$ and $p = 8.9 \times 10^{-7}$. When visualised as a scatter plot (Fig. 4d), a well demarcated threshold effect is observed at *ca.* 81% crystallinity (not too dissimilar to the discussion *vide supra* of the potential threshold effect at *ca.* 82% in the DoG *vs.* crystallinity data in Fig. 4b); above 81% crystallinity, the IEC remains consistent around 2.6 ± 0.1 mmol g^{-1}, whilst below this crystallinity threshold the IEC varies significantly and trends to higher values. The variances in IEC for sub-sample repeats with roll 1 were noticeably high (due to the use of the older MET titration method with this roll).

Fig. 5 shows the relationship observed between DoG and IEC for all the samples taken, as compared to theoretical IEC values (dashed blue line). A positive relationship is expected between DoG and IEC, a result of more functional groups being attached to the back bone and consequently more sites available for exchange.[29–31] This relationship plateaus at higher DoG values as IEC approaches the limit of the value that would be achieved with pure non-grafted poly(vinylbenzyltrimethyl-ammonium chloride) homopolymer, as shown in eqn (6):

$$\mathrm{IEC_{calc}} = \frac{1}{\frac{M_{\mathrm{VBC}}}{\left(\frac{\mathrm{DoG}}{100}\right)} + M_{\mathrm{VBC}} + M_{\mathrm{N(CH_3)_3^+}} + M_{\mathrm{Cl^-}}} \quad (6)$$

where M = molar mass per g per mol of the species indicated by the subscript.

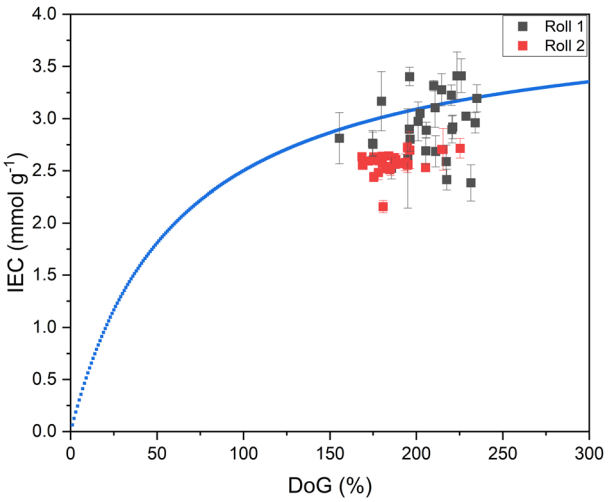

Fig. 5 The relationship between DoG and IEC with the dashed blue line showing the theoretical values, the black data points showing values from roll 1, and the red data points showing values from roll 2.

As the samples from both roll 1 and 2 had high DoG values of >160% only a weak positive relationship (Pearsons *R* value = +0.3) was observed between DoG and IEC. As seen on Fig. 5, the majority of the measured IEC values were below the theoretical value; this is expected as side reactions such as minor crosslinking between VBC grafted chains can occur, as previously discussed.[24,32]

AEM properties are interrelated, a good example of this was shown by Zhao *et al.*, where they demonstrated that simply changing the DoG impacts the micro- and nano-phase of the AEM which subsequently impacts IEC, hydration number and conductivity.[33] Hence, the in-plane conductivities and WUs were measured for all the RG-AEM samples in this study. Fig. 6a shows a moderate negative relationship (Pearsons *R* value = −0.6) was observed between a samples base film crystallinity and the resulting Cl^- conductivity; as the base film crystallinity increased, the DoG and IEC decreased and consequently the number of ionic groups available to participate in ionic conductivity decreased. Again, there was a reoccurrence of a threshold effect above *ca.* 81% crystallinity (clearly matching that seen in Fig. 4d when IEC is plotted against crystallinity). This is the key finding of this study: if the crystallinity of the HDPE films can be controlled to be above 81% (*e.g.* during production) then this will yield RG-AEMs with much more reliable properties (although there is a small conductivity penalty in obtaining this consistency).

A strong positive relationship was observed between crystallinity and WU (Pearsons *R* value = +0.7), where increased crystallinity resulted in increased water uptake (Fig. 6b). This relationship was unexpected as increased crystallinity was shown to decrease IEC and consequently reduce the number of hydrophilic cationic head groups.[34] The increase in WU may indicate that increases in degree of crystallinity values are not the whole picture, *i.e.* there could be concomitant changes to the shape, size, and distributions of the crystallites, leading to

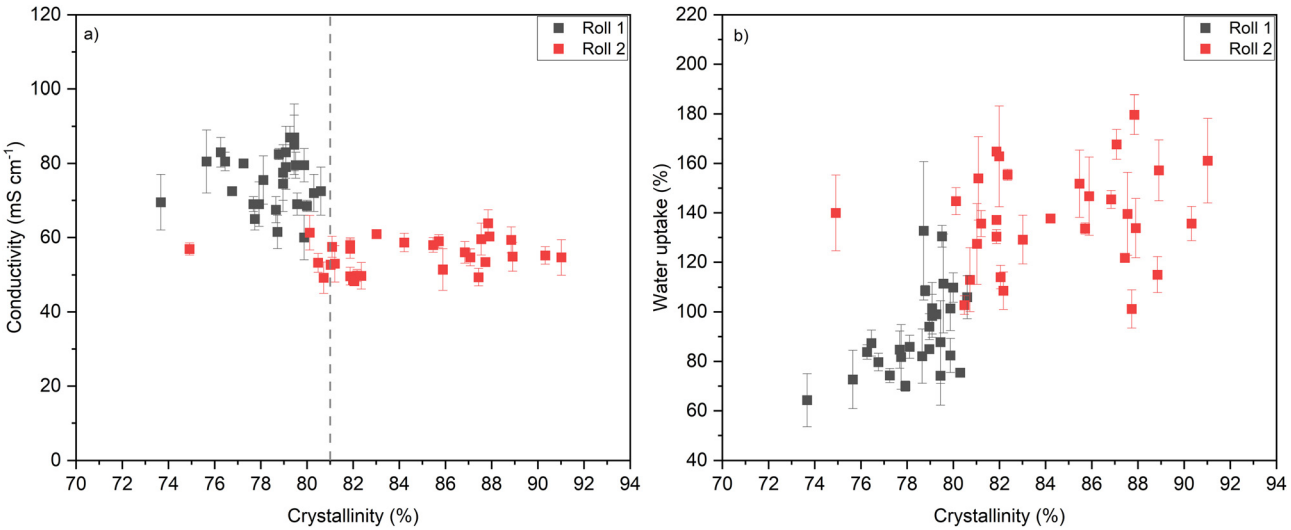

Fig. 6 (a) Scatter plot showing the relationship between crystallinity and conductivity where the black squares indicate values from roll 1 and the red squares shows values obtained from roll 2. The dashed line at 82% marks the threshold at which crystallinity appears to no longer impact conductivity. (b) Scatter plot showing the relationship between crystallinity and WU where the black squares indicate values from roll 1 and the red squares shows values obtained from roll 2.

more developed hydrated channels in the RG-AEM. Larger WU values can lead to excessive swelling, which can contribute towards reduced conductivities. This will need to be explored in more detail in a planned future study where crystallinity levels will be deliberately controlled.

Conclusions

The variation in crystallinity of a commercially supplied HDPE film from Goodfellows was measured using density measurements. Variations in the manufacturing process were shown to cause both inter- and intra-roll changes to the crystallinity, with degree of crystallinities ranging from 74–91%. This variation in degree of crystallinity of the precursor film was shown to impact the subsequent grafting and amination stages of RG-AEM production.

A negative correlation was demonstrated between HDPE crystallinity and degree of grafting (DoG, $R = -0.5$); this aligns with the literature, which shows that radiation grafting reactions dominate in the amorphous regions.[27,28] A negative correlation between crystallinity and ion-exchange capacity (IEC) and crystallinity and conductivity was also shown, with $R = -0.4$ and -0.6, respectively. A threshold effect was noted for DoG values, IECs, and conductivities at crystallinity values >81%; above this value the variations in the AEM properties were minimal with further increases in crystallinity. This suggests that to improve consistency of the properties of RG-AEMs, vital for scale-up, it is beneficial to direct the crystallinity of the base (precursor) film to values greater than such a threshold; we acknowledge that this threshold may be different with different HDPE suppliers, so this is something that researchers should keep in mind.

Finally, the relationship between water uptakes (WU) and crystallinity was examined. It was expected that increased crystallinities (shown to have reduced IECs and conductivities) would lead to lower WUs, due to the reduced number of hydrophilic cationic head groups. However, this was not the case and a positive relationship between crystallinity and WU was observed. This suggests that additional factors alongside raw degrees of crystallinity, such as crystallite size and distribution, may be directing the formation of the hydrophilic channel networks that are formed during the synthesis process. Further work is needed to understand this additional level of complexity.

Author contributions

The experiments were all conducted by Siân Franklin (PhD student). Siân Franklin conducted most of the data analysis with the assistance of John Varcoe (primary supervisor) and Carol Crean (co-supervisor). Siân Franklin drafted the bulk of the manuscript, while all authors provided comments and corrections.

Conflicts of interest

There are no conflicts to declare.

Data availability

The raw data behind the figures are available under a CC-BY open access licence at https://doi.org/10.6084/m9.figshare.29561156.

Supplementary information (SI): Raman cross-sectional analysis and SEM/photographic images of the surfaces of a RG-AEM sample. See DOI: https://doi.org/10.1039/d5lp00277j.

Acknowledgements

Siân Franklin's PhD project was kindly funded by AFC Energy Plc. The HDPE films and other lab consumables used were provided by funds from EPSRC grant EP/T009233/1. SEM assistance provided by James Whitting.

References

1 G. Das, J. H. Choi, P. K. T. Nguyen, D. J. Kim and Y. S. Yoon, *Polymers*, 2022, **14**, 1197–1232.
2 C. Li and J. B. Baek, *Nano Energy*, 2021, **87**, 106162–106180.
3 J. G. Hong, B. Zhang, S. Glabman, N. Uzal, X. Dou, H. Zhang, X. Wei and Y. Chen, *J. Membr. Sci.*, 2015, **486**, 71–88.
4 M. A. Hickner, A. M. Herring and E. B. Coughlin, *J. Polym. Sci., Part B:Polym. Phys.*, 2013, **51**, 1727–1735.
5 W. Lu, Z. G. Shao, G. Zhang, J. Li, Y. Zhao and B. Yi, *Solid State Ionics*, 2013, **245**, 8–18.
6 S. Maurya, S. H. Shin, Y. Kim and S. H. Moon, *RSC Adv.*, 2015, **5**, 37206–37230.
7 H. W. Zhang, D. Z. Chen, Y. Xianze and S. B. Yin, *Fuel Cells*, 2015, **6**, 761–780.
8 L. Wang, J. J. Brink, Y. Liu, A. M. Herring, J. Ponce-Gonzalez, D. K. Whelligan and J. R. Varcoe, *Energy Environ. Sci.*, 2017, **10**, 2154–2167.
9 W. H. Lee, C. Crean, J. R. Varcoe and R. Bance-Soualhi, *RSC Adv.*, 2017, **7**, 47726–47737.
10 L. Wang, X. Peng, W. E. Mustain and J. R. Varcoe, *Energy Environ. Sci.*, 2019, **12**, 1575–1579.
11 C. Rodriguez, B. Joensen, A. Moss, G. Larrazabal, D. Whelligan, B. Seger, J. Varcoe and T. Wilson, *ACS Sustainable Chem. Eng.*, 2023, **11**, 1508–1517.
12 V. Sproll, G. Nagy, U. Gasser, J. P. Embs, M. Obiols-Rabasa, T. J. Schmidt, L. Gubler and S. Balog, *Macromolecules*, 2016, **49**, 4253–4264.
13 M. Mamlouk, J. A. Horsfall, C. Williams and K. Scott, *Int. J. Hydrogen Energy*, 2012, **37**, 11912–11920.
14 K. Mortensen, U. Gasser, S. A. Gursel and G. G. Scherer, *J. Polym. Sci., Part B:Polym. Phys.*, 2008, **46**, 1660–1668.
15 H. P. Brack, H. G. Buhrer, L. Bonorand and G. G. Scherer, *J. Mater. Chem.*, 2000, **19**, 1795–1803.
16 N. Walsby, F. Sundholm, T. Kallio and G. Sundholm, *J. Polym. Sci., Part A:Polym. Chem.*, 2001, **39**, 3008–3017.
17 A. G. Biancolli, S. Bsoul-Haj, J. C. Douglin, A. S. Barbosa, R. R. de Sousa Jr., O. Rodriques, A. J. C. Lanfredi, D. R. Dekel and E. I. Santiago, *J. Membr. Sci.*, 2022, **641**, 119879–119891.
18 A. S. Barbosa, A. G. Biancolli, B. P. S. Santos, J. J. Bonvent, D. Hermida-Merino and E. I. Santiago, *React. Funct. Polym.*, 2025, **208**, 106149–106161.
19 K. Dawes, L. C. Glover and D. A. Vroom, in *Physical properties of polymers handbook*, Springer, New York, 2007, pp. 867–887.
20 M. M. Nasef, H. Saidi, K. Zaman and M. Dahlan, *Radiat. Phys. Chem.*, 2003, **68**, 875–883.
21 E. M. W. Tsang, Z. Zhang, A. C. C. Yang, Z. Shi, T. J. Peckham, R. Narimani, B. J. Frisken and S. Holdcroft, *Macromolecules*, 2009, **42**, 9467–9480.
22 Y. Zhao, K. Yoshimura, A. Radulescu and Y. Maekawa, *Macromolecules*, 2025, **58**, 663–671.
23 Z. Bartczak, *Polym. Test.*, 2018, **68**, 261–269.
24 L. Wang, E. Magliocca, E. L. Cunningham, W. E. Mustain, S. D. Poynton, R. Escudero-Cid, M. M. Nasef, J. Ponce-Gonzalez, R. Bance-Souahli, R. C. T. Slade, D. K. Whelligan and J. R. Varcoe, *Green Chem.*, 2017, **19**, 831–843.
25 Y. Hu, Y. Liao, Y. Zheng, K. Ikeda, R. Okabe, R. Wu, R. Ozaki, J. Xu and Q. Xu, *Polymers*, 2022, **14**, 3646–3655.
26 D. Mileva, D. Tranchida and M. Gahleitner, *Polym. Cryst.*, 2018, **1**, 1–16.
27 T. Motegi, M. Omichi, Y. Maekawa and N. Seko, *Radiat. Phys. Chem.*, 2024, **214**, 111281–111287.
28 X. Xie, X. Ling, F. Tian and Z. Tank, *Colloids Surf., A*, 2024, **700**, 134755–134763.
29 M. M. Nasef, H. Saidi, H. M. Nor and O. M. Foo, *Polym. Int.*, 2000, **49**, 1572–1579.
30 R. Espiritu, M. Mamlouk and K. Scott, *Int. J. Hydrogen Energy*, 2016, **41**, 1120–1133.
31 Z. Feng, G. Gupta and M. Mamlouk, *Int. J. Hydrogen Energy*, 2023, **48**, 25830–25858.
32 T. Yamaki, K. Kobayashi, M. Asano, H. Kubota and M. Yoshida, *Polymer*, 2004, **45**, 6569.
33 Y. Zhao, K. Yoshimura, A. Radulescu and Y. Maekawa, *Macromolecules*, 2025, **58**, 663.
34 J. L. Di Salvo, G. De Luca, A. Cipollina and G. Micale, *J. Membr. Sci.*, 2020, **599**, 117837.